Crosstalk in Polymer Microelectrode Arrays

Yi Qiang^{1,5}, Wen Gu^{1,5}, Zehua Liu¹, Shanchuan Liang¹, Jae Hyeon Ryu¹, Kyung Jin Seo¹, Wentai Liu² and Hui Fang^{1,3,4,*}

¹Department of Electrical and Computer Engineering, Northeastern University, Boston, MA 02115, USA

² Department of Bioengineering, University of California, Los Angeles, Los Angeles, CA 90095, USA

³Department of Bioengineering, Northeastern University, Boston, MA 02115, USA

⁴Department of Mechanical and Industrial Engineering, Northeastern University, Boston, MA 02115, USA

⁵*These authors contributed equally to this work.*

Keywords: crosstalk effect, flexible microelectrodes, equivalent circuit modelling, finite element analysis, polymer

^{*}Corresponding Author

Abstract

Thin-film polymer microelectrode arrays (MEAs) facilitate the high-resolution neural recording with its superior mechanical compliance. However, the densely packed electrodes and interconnects along with the ultra-thin polymeric encapsulation/substrate layers give rise to non-negligible crosstalk, which could result in severe interference in the neural signal recording. Due to the lack of standardized characterization or modeling of crosstalk in neural electrode arrays, to date, crosstalk in polymer MEAs remains poorly understood. In this work, the crosstalk between two adjacent polymer microelectrodes is measured experimentally and modeled using equivalent circuits. Importantly, this study demonstrated a two-well measuring platform and systematically characterized the crosstalk in polymer microelectrodes with true isolation of the victim channel and precise control of its grounding condition. A simple, unified equation from detailed circuit modeling was proposed to calculate the crosstalk in different environments. Finite element analysis (FEA) analysis was conducted further to explore the crosstalk in more aggressively scaled polymer electrode threads. In addition to standardizing neural electrode array crosstalk characterization, this study not only reveals the dependence of the crosstalk in polymer MEAs on a variety of key device parameters but also provides general guidelines for the design of thin polymer MEAs for high-quality neural signal recording.

1. Introduction

Thin-film polymer microelectrode array (MEA) has emerged as an increasingly important device in neuroscience and neural engineering by enabling the measurement of neuronal activities through a more mechanically compliant substrate to the soft tissue[1-3]. For example, researchers at *Neuralink* have recently developed flexible electrode "threads" with over thousands of electrodes, which can be implanted into the brain and target specific brain regions for signal recording[4]. Continued research on the polymer MEA, which includes higher electrode densities, larger channel count, and better-optimized encapsulation/substrate layers and device footprint, is essential for achieving the desired performance, such as its spatial resolution, signal quality, information throughput, and chronic biocompatibility [5-8]. However, densely packed, ever-increasing numbers of microelectrodes and interconnects in scaled MEAs will lead to signal crosstalk, which can cause severe interference in the signal recording[9]. In the state-of-art silicon (Si)-based neural probe design, the crosstalk coefficient ranging from 0.006% to 8% has been reported, while crosstalk larger than 1% is considered as non-negligible in the neural signal recording[10-17]. The situation could be even worse for polymer MEAs, due to the limited insulation properties of polymer materials and thin encapsulation/substrate layers they require to achieve the mechanical compliance. While there has been existing crosstalk studies on Si-based neural devices, crosstalk was rarely reported in polymer MEAs. Moreover, how different device parameters affect the crosstalk in polymer MEAs remains also largely unknown to date.

In literature, different methods are adopted to analyze the crosstalk in Si probes. Equivalent circuits of two parallel metal traces have been developed in multiple studies for analyzing the crosstalk in Si probes[11, 12]. In those circuit models, crosstalk can be theoretically modeled by considering the different impedances involved in the recording path, such as the electrode impedance, amplifier input impedance, trace shunting impedance and the

most important, coupling impedance between the lines. These impedances can be measured experimentally to derive the crosstalk[9]. Crosstalk can also be experimentally quantified by having electrical signals input to one channel and recording from the adjacent channel[10, 12]. However, due to the lack of a local micro-scale signal generator (a bench-test equivalent to a neuron), it has been challenging to measure the exact crosstalk values from real devices or test structures and validate the accuracy of the crosstalk circuit modeling. Moreover, different studies have quantified crosstalk in different individual environments, such as in the air or a saline solution. However, none of the prior studies have considered the fact that the crosstalk is affected by different electrode grounding conditions and included this consideration into the modeling and characterization towards the more accurate prediction of crosstalk *in vivo*. Specifically, in real *in vivo* settings, the victim electrodes are not grounded or encapsulated by insulators like in typical Si probe studies due to that they are also meant to record neuronal signals. In general, there is no standardized characterization or modeling of crosstalk in neural electrode arrays, regardless of their types.

In this work, we holistically studied the crosstalk between adjacent microelectrodes in a thin Kapton thread from cross-examining newly-enabled theoretical and experimental results. First, with a novel two-well, three-environment setup, we systematically measured the crosstalk between two flexible microelectrodes with true isolation of the victim channel from the signal input from the two wells, and as a function of different interconnect distances, different thicknesses of the SU8 encapsulation layer, as well as different grounding conditions the victim channel is placed in, namely dry, floating wet and wet with varying shunt impedances. We then modeled the crosstalk by equivalent circuits under a unified framework using the coupling impedance between electrodes and their interconnects, which was further validated by the frequency dependence of the experimental crosstalk results from the two-well setup and three different environments. We further leveraged Finite Element Analysis (FEA) to simulate the

coupling impedance between electrodes and their interconnects and predicted the crosstalk in more aggressively scaled polymer MEAs at *in vivo* settings as a function of key device parameters. This study not only standardizes the crosstalk evaluation for general MEAs but also specifically sheds light on the dependence of the crosstalk in polymer MEAs on a variety of important device parameters and provides the guidelines to the design of polymer MEAs for high-quality neural interfaces.

2. Results and discussion

2.1. The Two-Well Setup

To investigate the crosstalk from electrodes on polymer MEAs, we fabricated two adjacent microelectrodes on a Kapton substrate with SU8 encapsulation as a model system. Poly(3,4-ethylenedioxythiophene) polystyrene sulfonate (PEDOT:PSS) was electro-deposited on the Au electrode site to reduce the site impedance to values relevant to practical neuroelectrodes. The lengths of the interconnect of the two model electrodes are different to isolate the input signals to only one of them. The two electrodes were then placed into a customized measurement platform to measure the crosstalk (Figure 1a, b). The measurement platform consists of two polycarbonate wells, with O-rings placed on the top of the well to prevent any leakages when containing liquid solutions. Figure S1 in ESM shows optical images of the measurement setup. Although crosstalk from Si probes and circuit modeling has been widely reported in previous studies, the measurement often incurs fabrication of test devices with the victim channel electrodes encapsulated or grounded, which miss-counted the coupling from the electrode site impedance. However, as a matter of fact, the victim electrode is also functional in the real *in vivo* settings, not grounded or encapsulated. The crosstalk values are also reported either in air ambient or saline without consistent standards regarding the victim-electrode grounding[11, 12]. The customized two-well platform in the present study enables measuring the crosstalk with true isolation of the victim channel from the signal input and precise control of its grounding condition separately. Specifically, as shown in Figure 1a, the electrode with a shorter trace (victim trace) resided in Well 1, and the electrode with a longer trace (aggressor trace) was inside Well 2. The length of the trace overlap is fixed to be 14 mm for this study, while the two wells have the same diameters of 14.5 mm to contain the major trace overlap in Well 2. The length of trace overlap outside the Well 2 did not exceed 1 mm throughout the measurement to ensure the accuracy of the result. Test signals were input into Well 2 while both contact pads of the two electrodes were connected to different channels of the data acquisition system (DAQ). As only the site of the aggressor electrode was inside Well 2, the output from the victim electrode will not include the input signals but only the crosstalk from the aggressor electrode. The overlapping part of two electrode traces is primarily placed in Well 1, where its environment can be controlled from different grounding. The site area is $6400 \,\mu\text{m}^2 \,(80 \times 80 \,\mu\text{m}^2)$ for both microelectrodes, while the gap between the two traces and the thicknesses of SU8 layer are varied to examine their effects. The impedance of the electrode is about 10 k Ω after PEDOT: PSS coating. Data acquired from the pad connected with the victim trace therefore yields the crosstalk signal in controlled environments (Figure 1c). Characterizing the crosstalk effect of high-density, multi-electrode arrays using electrical signals is challenging considering the electrode spacings which are usually too small to isolate the input to a single channel. Thus, determining crosstalk effect using the simple 2-trace system with the 2-well measuring platform will be helpful in predicting the crosstalk for the real devices and guiding the device design. The 2-well platform can also be customized to test the devices with different shapes such as the ones with curved or multi-crossed interconnects.

In this study, we have investigated the crosstalk effect in environments of dry, floating wet, and wet with shunt conditions, respectively, where dry environment means the medium in Well 1 is air while floating wet environment indicates there is PBS solution in Well 1 with floating ground. If the PBS solution in Well 1 is connected to the ground through certain resistance (Z_{sh}), we name it as wet with shunt condition. These three different environments

cover all the grounding scenarios a microelectrode might experience during signal recording from the bench testing to *in vivo* settings. Therefore, measuring the crosstalk from all three environments is important to derive the comprehensive crosstalk information from the devices.

Specifically, crosstalk in dry condition is measured when the victim electrode and interconnects are placed in air ambient. In the *in vivo* setting, this scenario can resemble crosstalk from the non implanted electrodes. While theoretically being an open circuit, non-implanted electrodes may record similar neural signals as in implanted ones if there is a strong crosstalk effect. Crosstalk in floating wet condition is measured when the victim electrode and overlapping interconnects are immersed in PBS solution with no ground connections (floating ground). For *in vivo*, it represents the crosstalk from the implanted electrodes with no or poor grounding connections made on the implanting model. The last environment, namely the wet condition with a shunt is really designed to mimic the realistic in vivo recording environment, where the electrodes are operating in wet tissue with a certain impedance between the victim trace electrode and the ground[18, 19]. Notably, the wet with shunt condition also includes the circuit components in dry conditions, as certain devices may have densely-packed interconnects that will be left outside the tissue during the recording.

2.2. Equivalent circuits

To understand the crosstalk from the two-well measurements, we performed an equivalent circuit analysis of the three different environments in Well 1. The equivalent circuit elements include the intrinsic coupling impedance between the two electrode traces inside the encapsulation layer (Z_{dry}), the impedance from electrode trace to the wet medium through the encapsulation layer (Z_{wet}), electrode site impedance (Z_s), amplifier input impedance (Z_{in}) and shunt impedance (Z_{sh}). Solution resistance (Z_{sol}) is also included but considered negligible in the circuit modelling. The equivalent circuits for the three environments are different, as shown in **Figure 2a** and **2b**, resulted from these different electrical settings. Here, the definition of the

crosstalk is the root mean square (RMS) of output signal amplitude (V_{o2}) from the victim trace divided by the RMS of input signal amplitude to the aggressor trace (V_{i1}). Simplified equations from the equivalent circuits for calculating crosstalk are summarized in **Figure 2c**. The assumption here includes a much smaller electrode site impedance (Z_s) compared to the Z_{wet} and Z_{in} . Interestingly, the equations of all three environments can be unified under the coupling impedance (Z_s) between the two electrodes and their interconnects in Well 1, as below.

$$Crosstalk = \frac{Z_{in}||Z_{sh}}{Z_{in}||Z_{sh} + Z_c}$$
 (1)

Here Z_c represents different circuit elements in the three different environments (**Figure 2c**). In the dry environment, this coupling impedance only originates from the SU8 encapsulation layer and the two electrode traces in Well 1; thus Z_c equals to Z_{dry} (assuming that the impedance from the air is infinite). While in the other two environments, Z_c is contributed not only from Z_{dry} , but also from the additional impedances due to the surrounding PBS solution, which includes the Z_{wet} and Z_s , the latter of which can be neglected with high-performance MEAs. Z_c can be experimentally measured using a potentiostat with a two-electrode configuration, while the input impedance (Z_{in}) comes from the data acquisition system and can be measured too. Z_c highly depends on the encapsulation layer and device substrates, including the types and thicknesses of the materials. If Z_s and Z_{sh} are both non-negligible, the circuit result will become more complicated than **Equation 1** and the crosstalk value will eventually be influenced by both of these two values.

It's also worthwhile to note that the circuit modeling here is also applicable to other MEAs, such as conventional Si probes. Compared to the circuit modeling in previous work, here we considered for the first time victim electrode shunt paths and their changes from different grounding conditions to study the crosstalk effect. While some of the previous work modelled the recording path with victim channel grounded and derived the simplified crosstalk equations for the Si probes[11, 12], the circuit modelling and hence the crosstalk value will be

significantly different if a non-negligible shunt impedance (Z_{sh}) is present, which is likely the case *in vivo*. Thus, we propose the circuit modelling in wet with shunt condition should be adopted as the standard for characterizing the *in vivo* crosstalk of general microelectrode arrays since all the necessary circuit elements in the real *in vivo* setting are considered and well-placed. In this study, we also experimentally validated this victim-shunt-incorporated crosstalk modeling through changing the different grounding conditions and shunt resistances in Well 1 which hosted the victim electrode, as shown in the following analysis.

2.3. Crosstalk analysis

To quantify the crosstalk in polymer MEAs and understand its physics, the crosstalk measured from the two-well setup and modeled from the equivalent circuits was compared. The electrode with the longer interconnect (aggressor trace) was connected to the working electrode while the electrode with the shorter interconnect (victim trace) was connected to the counter electrode to measure the total coupling impedance (Z_c) in both dry (air in Well 1) and wet (PBS in Well 1) environments. The input impedance Z_{in} was measured to be 13 M Ω consistently in the Intan recording system, which we leveraged as the data acquisition system to measure signals. Impedance was always measured at 1 kHz if not specified. Impedance at 1 kHz has been widely accepted for characterizing neural electrodes[20, 21]. Z_{sh} was added to the measuring system using DC resistors from 47 k Ω to 2 M Ω , which covers a wide range of the *in vivo* microelectrode shunt impedance to the ground[22]. For all three environments, the measured and calculated crosstalk reveals high consistency with each other across a wide band of frequencies from 1 Hz to 5000 Hz. While it might not be an apparent trend for dry and wet environments, the frequency dependence of the crosstalk can be clearly observed when the shunt impedance is included in the system (**Figure 3a, b**). The crosstalk increases with both

higher frequency and higher shunt impedance, indicating the threat of the crosstalk effect rises with higher-frequency band signal recording and poorer grounding.

These dependencies on both shunt impedance and frequency can be explained by the equivalent circuit models we have developed (Figure 2). For shunt, if assuming Z_{sh} is much smaller than the input impedance Z_{in} , the crosstalk equation can be further simplified to $1/(1+Z_c/Z_{sh})$, which is consistent with the observed trend – higher Z_{sh} leading to increasing crosstalk. This trend implies the significance of having a low-impedance path from the microelectrodes to the ground in terms of decreasing the crosstalk effect. On the other hand, the circuit elements in the crosstalk equation, namely Z_{in} and Z_c , are both frequency-dependent. Z_{in} originates from the parasitic capacitance in the amplifier circuits, thus is inversely proportional to the frequency [23]. Z_c is more complicated and environment-dependent. Experimental results indicate that Z_c in both dry and wet environments are highly capacitive, as the exponents of the fitting curves in Figure 3c are both close to -1. Overall, our circuit modeling demonstrates good consistency with the experimental results for crosstalk in all three environments and in a wide range of frequency, validating the accuracy of the crosstalk modeling using the proposed unified equation. In the device design, if one can measure or simulate the coupling impedance Z_c and is aware of the values of Z_{in} and Z_{sh} , the crosstalk in all three environments can then be calculated. Since the desired parameters are not difficult to derive, the proposed crosstalk modeling can provide designers with the convenience and guidance to probe into the crosstalk effect at the device design stage.

We further investigated how parameters such as the gap between neighboring interconnect and encapsulation layer thickness affect the crosstalk. As is known, device parameters can have a substantial influence on the crosstalk. To this end, we fabricated electrodes with different gaps between their interconnects ranging from 5 to 40 μ m and different SU8 encapsulation thicknesses from 5 to 20 μ m. The gap between the two traces exhibits a

different impact on the crosstalk in dry and wet environments (Figure S2a in ESM). The crosstalk in the dry environment decreases with larger gaps due to a larger Z_{dry} , consistent with the modeling, as Z_{dry} is highly capacitive. Meanwhile, we observed minimal change of the crosstalk in wet environments with various gaps, both with and without a shunt. This is also expected from our crosstalk equation since the total coupling impedance (Z_c) in this case is dominated by the impedance from electrode traces to the PBS solution (Z_{wet}), due to the much larger Z_{dry} in parallel and negligible solution impedance (Z_{sol}) in series. Since Z_{wet} is mainly related to the thickness of the encapsulation layer, the crosstalk is not expected to change significantly with just the gap variation (Figure S2a in ESM). On the other hand, crosstalk shows opposite trends in dry and wet environments as a function of the SU8 thicknesses (Figure **S2b in ESM**). For the dry environment, Z_{dry} decreases with a thicker SU8 layer, though only slightly, due to a larger capacitance between the traces from the fringing effect within the thicker SU8 layer, which eventually results in larger crosstalk. However, in wet environments both with and without a shunt, Z_{wet} becomes larger with a thicker SU8 layer insulating the electrode traces due to decreased parallel-plate capacitance. The increase in Z_{wet} leads to smaller crosstalk in wet environments due to a larger coupling impedance Z_c (Figure S2c in ESM). In our measurements, the crosstalk in the floating wet environment has been the largest among all three environments. With a 10 µm gap and 5 µm SU8 thickness in our test devices, the crosstalk can reach 56% at 1 kHz in the floating wet condition, while the value of the other two environments stays below 20% (Figure S2b), showing clear differences. When the shunt impedance is included, the crosstalk becomes dependent on the given shunt impedance value, which can be even smaller than the crosstalk in dry condition if the shunt impedance is small. As we mentioned, in the real in vivo recording, the circuit scenario is closest to the wet with shunt condition, as the animals are usually grounded with external/internal reference electrodes that are not far away from the electrodes and some interconnect. Therefore, the shunt impedance from electrodes to the ground plays an important role in determining the crosstalk value.

2.4. Simulation of the coupling impedance and crosstalk prediction

Flexible MEAs are now fabricated with highly scaled form factors, ultra-thin polymer layers and aggressive feature sizes to achieve better mechanical compliance to the tissue and higher density of electrodes. Though having the size and pitch of the electrodes comparable to the size of neurons (usually over 10 µm) is sufficient for achieving single-unit recording, it is necessary to scale the electrode interconnects to even sub-micron levels for realizing MEAs with high density and large throughput. State-of-art polymer MEAs with high densities and flexibility achieved electrode interconnects and spacings from 0.2 to 2 µm and polymer thicknesses both as the substrate and encapsulation layers from 0.8 to 2 µm[4, 24, 25]. Polymer MEAs have limited insulation capability from the polymer substrate and encapsulation layers compared to Si, silicon oxides, and nitrides, which are used to protect the Si-based MEAs[11]. Polymers such as Polyimide, Polydimethylsiloxane (PDMS), and Parylene C are also known for the degradation of insulation properties in long-term studies[26-28]. As a result, polymer MEAs are facing a more significant threat from crosstalk than the Si-based devices during scaling and miniaturization.

To predict the crosstalk in polymer MEAs as they scale, it is highly beneficial to simulate the coupling impedance Z_c . In this work, we utilized the COMSOL 5.2a Finite Element Analysis (FEA) software to conduct a series of simulations. A 2D model with customized mesh sizes was adopted, consisting of two electrode traces, the encapsulation layer, the substrate layer, and a large circular ambient with infinite element domain at the outer boundary (**Figure S3 in ESM**). The simulation protocol is to tie the input voltage to one electrode trace and ground one end of the other electrode trace. In this way, we can derive the electrostatic potential around the electrodes (**Figure 4a**). The coupling capacitance between the two traces was then derived and used to calculate the crosstalk in different environments. The microelectrode site impedance is assumed to be negligible in this simulation since the site impedance of high-performance MEAs

is normally much smaller than the coupling impedance (In our fabricated devices, averaged microelectrode impedance is $10 \text{ k}\Omega$ at 1 kHz, while the typical value of coupling impedance is over $5 \text{ M}\Omega$). The accuracy of this simulation model was validated with the device parameters adopted in the previous experiments. Here, the model accuracy is defined as below:

$$Model\ Accuracy = 1 - \frac{|c_{sim} - c_{exp}|}{c_{exp}} \tag{2}$$

where C_{sim} represents the simulation-derived crosstalk, and C_{exp} refers to the experimental results.

The simulated crosstalk as a function of trace gaps and SU8 thicknesses shows similar value and trends with the experimental results, with an overall model accuracy above 90% (Figure 4b, c). The model accuracy deviates with smaller gaps due to the inaccurate computation at the model edges in the FEA analysis. A finer mesh size will increase the model accuracy but will elongate the simulation time. More detailed validation results, including the crosstalk simulation with various shunt impedances, can be found in Figure S4 in ESM.

To further validate the accuracy of our crosstalk prediction at the nanoscale, we also sampled reported crosstalk values from state-of-the-art Si-based MEAs and conducted crosstalk simulation using their device parameters and the model developed here (**Figure 4d**). As details are shown in **Table S1 in ESM**, the simulated crosstalk results are comparable to the reported values, but some are with certain discrepancies. The accuracy of the simulation can be further improved by knowing more specific information from the reported devices. Also, in the simulation model, the device structure of the Si probes is usually simplified. The variations in the device parameters, structures and even adopted material properties could certainly cause the discrepancies in the simulations.

With the confidence from the high model accuracy, we simulated the crosstalk with the change of trace gaps, SU8 thicknesses, and trace widths using nanoscale parameters. The selected trace gaps, SU8 thicknesses, and trace widths are from 0.1 to 1 μ m, 0.15 to 1 μ m, and

0.1 to 2 µm, respectively. The length of electrode traces is fixed to be 10 mm. All of these parameters are chosen based on the literature reporting state-of-art Si-based MEAs fabricated with complementary metal-oxide-semiconductor (CMOS) technologies [10, 13, 14]. Unlike the weak dependence in less-scaled devices, the crosstalk in scaled devices increases significantly with decreasing trace gaps for all dry, floating wet, and wet with shunt environments (**Figure 4e**), since Z_{wet} is now comparable to Z_{dry} , not dominating Z_c anymore. The blue area with two dashed line boundaries in Figure 4e displays the fluctuation of the crosstalk with different shunt impedances ranging from 0.5 M Ω to 10 M Ω . Clearly, better grounding is highly beneficial for reducing the crosstalk in scaled MEAs. The SU8-encapsulation thickness dependence is also different than that of the less-scaled devices, mainly in wet conditions. Specifically, the crosstalk remains largely the same before the encapsulation gets ultra-scaled (in our simulation conditions, less than 300 nm), where a thinner SU8 layer increases the crosstalk in wet environments (both with and without a shunt) (Figure 4f). This invariance could be attributed to the opposite changes in Z_{dry} and Z_{wet} , which are at similar orders, with Z_{dry} increasing with the thinner insulation due to the fringing effect and Z_{wet} decreasing because of a larger capacitance between the trace and the wet medium. Ultimately Z_{wet} would dominate in the parallel network since it's smaller, and its continued decrease as encapsulation thinning will lead to crosstalk rising. Some other device parameters have also been studied using the simulation model. For example, reducing the interconnect trace widths decreases the crosstalk in all three environments, as shown in **Figure 4g**, due to less fringing capacitance introduced. Larger Au layer thicknesses (from 50 to 300 nm) increase crosstalk (Figure 4h), while the change of Polyimide substrate thickness from 1 to 25 µm does not worsen the crosstalk (Figure 4i) at a given SU8 thickness of 500 nm, as the coupling impedance is dominated by the insulation layer.

Finally, we conclude and propose the following guidelines on key device parameters around current fabrication feature sizes to minimize the crosstalk in scaled MEAs, especially

those polymer ones. We note that these guidelines are primarily from minimizing the crosstalk perspective at *in vivo* settings and should be cross considered with other desires in device performance, too, such as the electrode impedance, density, and chronic performance, *etc*.

- 1. A highly important design consideration, perhaps more effective than tuning the device dimensional parameters in minimizing the crosstalk, and more critical in polymer MEAs than in Si probes, is to have proper electrode grounding, to minimize the victim channel's shunt impedance and its influence. Local and even multiple grounds should be utilized for high-throughput devices with multiple electrodes.
- 2. While it is conventional to have low electrode impedance in high performance MEAs, there are still controversies in whether impedance matters in neuronal recording[29]. The guideline above also indicates that low electrode impedance is still important, now for achieving small crosstalk, in addition to low noises. High electrode impedance is simply equivalent to poor grounding.
- 3. From the interconnect and electrode density point of view, narrower interconnect width will lead to less crosstalk from reduced parallel-plate capacitance, thus is to the advantage of scaling, but narrower interconnect gap will increase crosstalk from elevated fringing capacitance. Eventually, one could co-scale the interconnect width and gap during electrode array scaling while not be penalized in the crosstalk.
- 4. Decreasing interconnect thickness can serve as an effective means to reduce the crosstalk from decreasing the fringing capacitance between interconnect lines.
- 5. Surprisingly, scaling down of the encapsulation or substrate thickness, even to the deep sub-micron regime, will not increase the crosstalk significantly, if the electrodes are of sufficiently low impedance and have access to proper grounding. This thickness independence can be leveraged to significantly scale down the entire thickness of the probe to reduce the insertion footprint and therefore reduce the acute tissue damage and improve the chronic biocompatibility. Note that this thickness

scaling does have a limit when the interconnect impedance from the parallel plate coupling with the biofluid is approaching the channel shunt impedance.

3. Conclusion

In this work, we developed a novel two-well, three-environment platform, and holistically characterized the crosstalk in polymer MEAs with true isolation of the victim electrode. Equivalent circuit modeling unveiled the crosstalk effect originating from different circuit elements and generated a unified equation for calculating crosstalk in polymer MEAs under different electrode grounding conditions, namely dry, floating wet, and wet with a shunt. Systematic studies of the crosstalk in two adjacent electrode traces revealed that the crosstalk value matches well with the modeling in all different environments, validating our approach. Furthermore, we simulated the coupling impedance and predicted the crosstalk for nanoscale polymer MEAs, which provides the guidelines for designing thin-film polymer MEAs with minimal crosstalk. We propose here this coupling impedance-based crosstalk calculation in wet with shunt environment as the standard for characterizing the in vivo crosstalk of microelectrode array. We believe the crosstalk measurement and characterization demonstrated in this work is applicable to all polymer based MEAs and our conclusions can be extended to those devices as well. Future work will include the crosstalk dependence studies of different materials, longterm crosstalk characterizations of various polymer MEAs, as well as the device designs to reduce the crosstalk effect on polymer MEAs. We believe the study here not only standardizes the crosstalk evaluation for general MEAs but also provides general guidelines for the design of polymer MEAs specifically for high-quality neural interfaces.

4. Experimental Section

Materials and Tools: All the chemicals used in this work were purchased from Thermo Fisher Scientific. All materials were used as received. The impedance measurement was conducted

using Gamry Potentiostat 600+ (Gamry Instruments). Crosstalk signals were acquired with Intan RHD2164 amplifier and 512-ch recording controller (Intan Technologies). MATLAB R2019a (Mathworks, Inc) was used for data processing. Device simulation was completed using COMSOL 5.2a (COMSOL, Inc).

Device Fabrication: The fabrication began with the depositions of 5 nm of Cr and 70 nm of Au on the half-mil thick Kapton substrate, which were at the rates of 0.5 and 1 A/s, respectively. Photoresist (S1818, Shipley) spin-coated the Au layer using 3000 rpm for 30 s. Then, photolithography defined the electrode and interconnect patterns with UV exposure and development, followed by wet etching of Au and chromium layers with Au and chrome etchants, respectively. Acetone, isopropyl alcohol (IPA), and DI water removed the remaining photoresist. SU-8 2005/2010/2020 spin-coated the patterned Au electrodes using 3000 rpm for 30 s for contact area isolation. After soft baking at 95 °C for 2 min, UV exposed the SU-8 for 7 s, followed by a postexposure baking at 95 °C for 3 min. For development, sonication in SU-8 developer for 30 s and rinsing with fresh SU-8 developer and IPA yielded clear SU-8 patterns. Hard bake at 200 °C for 20 min finalized the process. The thickness of SU-8 was from 5 µm to 40 μm, with multiple time of SU8 spin-coating used for the thicknesses over 20 μm. The fabricated electrode had a 10 mm length, 100 μm width, and 2 mm × 2 mm contact pad size. PEDOT: PSS was then electroplated to the electrode surface for decreasing the impedance. We followed the electrodeposition process that has been described specifically in the previous work[30].

Crosstalk Measurement: The crosstalk measurement was conducted using the customized platform which includes 2 polycarbonate wells both with O-ring contact. The 2 electrodes were placed into the wells and secured using the O-rings on the top. The electrode site of the longer trace (Aggressor electrode) was placed in the well connected to the input sinewave signals provided by a Digilent function genarator (Digilent, Inc). The electrode site of the shorter trace (Victim electrode) was placed in the second well. PBS solution was used in both wells as the

medium to deliver the input signals and for the crosstalk measurement in wet environments. The contact pads of the 2 electrodes were connected to the Intan RHD 2164 amplifier and 512-ch Intan recording controller for data sampling with the sampling frequency at 20 kHz. The collected data were then analyzed in MATLAB R2019a software to calculate the crosstalk coefficients. A picture of measurement setup is shown in **Figure S1 in ESM** for details.

Impedance Measurement: Capacitance were derived with Gamry Potentiostat 600+ (Gamry

Instrument) using a 2-electrode environment. The 2 electrodes were placed into the customized platform same as the crosstalk measurement, with PBS solutions added to both wells. The working electrode was connected to the Aggressor electrode while the counter electrode was connected to the victim electrode, also shorted to the reference electrode. The Electrochemical impedance spectroscopy (EIS) was then conducted with sweeping frequency from 1 to 100 kHz with a 10 mV RMS AC voltage.

Device Simulation: The finite element analysis software simulated the coupling capacitance between 2 electrode traces in Micro/Nanoscale devices. A 2D simulation model was built with localized mesh sizes. The model includes a large, circular ambient wrapped with an infinite element domain, a layer of device substrate, 2 electrode traces and an encapsulation layer. While the mesh size for the ambient domain ranges from 10 to 100 μm, it narrows to a range from 0.01 to 0.5 μm in the device layers. An input of 1 V was applied though one of the electrode traces and the other electrode trace is grounded. The coupling capacitance was then computed using the model and converted to impedance afterwards. The crosstalk was then calculated using the equations in **Figure 2c**.

Electronic Supplementary Material: Supplementary material (Setup of crosstalk measurement; Measured crosstalk with variation of trace gaps and encapsulation layer thicknesses; FEA simulation model; Measured crosstalk with different shunt resistance; Summary of crosstalk studies of the state-of-the-art Si probes with simulated results.) is

Acknowledgements Y.Q. and W.G. contributed equally to this work. This work is supported by National Science Foundation award 1847215, National Institute of Neurological Disorders and Stroke award 1RF1NS118301-01 and Samsung Global Research Outreach Award. We acknowledge the use of the George J. Kostas Nanoscale Technology and Manufacturing Research Center at Northeastern University for device fabrication.

Author contributions Y.Q. and H.F. designed the research; Y.Q., W.G., J.H.R., K.J.S, fabricated the devices; Y.Q., Z.L., S.L., performed data analysis; Y.Q., W.G., W.L., and H.F. cowrote the manuscript.

Author information The authors declare no competing financial interests. Correspondence and requests for materials should be addressed to H.F. (h.fang@northeastern.edu).

References

- [1] Cheung, K. C.;Renaud, P.;Tanila, H.;Djupsund, K. J. B.; Bioelectronics Flexible polyimide microelectrode array for in vivo recordings and current source density analysis. *Biosensors and Bioelectronics* **2007**, *22*, 1783-1790.
- [2] Stieglitz, T.; Schuettler, M.; Meyer, J.-U. J. B. m. Micromachined, polyimide-based devices for flexible neural interfaces. *Biomedical microdevices* **2000**, *2*, 283-294.
- [3] Castagnola, V.;Descamps, E.;Lecestre, A.;Dahan, L.;Remaud, J.;Nowak, L. G.;Bergaud, C. J. B.; Bioelectronics Parylene-based flexible neural probes with PEDOT coated surface for brain stimulation and recording. *Biosensors and Bioelectronics* **2015**, *67*, 450-457.
- [4] Musk, E. J. J. o. m. I. r. An integrated brain-machine interface platform with thousands of channels. *Journal of medical Internet research* **2019**, *21*, e16194.

- [5] Shi, J.; Fang, Y. J. A. M. Flexible and implantable microelectrodes for chronically stable neural interfaces. *Advanced Materials* **2019**, *31*, 1804895.
- [6] Wang, J.; Zhao, Q.; Wang, Y.; Zeng, Q.; Wu, T.; Du, X. J. A. M. T. Self Unfolding Flexible Microelectrode Arrays Based on Shape Memory Polymers. *Advanced Materials Technologies* **2019**, *4*, 1900566.
- [7] Kaiju, T.; Yokota, M.; Watanabe, K.; Inoue, M.; Ando, H.; Takahashi, K.; Yoshida, F.; Hirata, M.; Suzuki, T. J. F. i. n. c. High spatiotemporal resolution ECoG recording of somatosensory evoked potentials with flexible micro-electrode arrays. *Frontiers in neural circuits* **2017**, *11*, 20.
- [8] Lee, M.;Shim, H. J.;Choi, C.; Kim, D.-H. J. N. l. Soft high-resolution neural interfacing probes: Materials and design approaches. *Nano letters* **2019**, *19*, 2741-2749.
- [9] Cruz, M. F. P.; Vomero, M.; Zucchini, E.; Delfino, E.; Asplund, M.; Stieglit, T.; Fadiga, L. Can Crosstalk Compromise the Recording of High-Frequency Neural Signals? In 2019 9th International IEEE/EMBS Conference on Neural Engineering (NER); IEEE, 2019; pp 924-927.
- [10] Herbawi, A. S.;Christ, O.;Kiessner, L.;Mottaghi, S.;Hofmann, U. G.;Paul, O.; Ruther, P. J. J. o. M. S. CMOS neural probe with 1600 close-packed recording Sites and 32 analog output channels. *Journal of Microelectromechanical Systems* **2018**, *27*, 1023-1034.
- [11] Rios, G.; Lubenov, E. V.; Chi, D.; Roukes, M. L.; Siapas, A. G. J. N. l. Nanofabricated neural probes for dense 3-D recordings of brain activity. *Nano letters* **2016**, *16*, 6857-6862.
- [12] Lopez, C. M.; Andrei, A.; Mitra, S.; Welkenhuysen, M.; Eberle, W.; Bartic, C.; Puers, R.; Yazicioglu, R. F.; Gielen, G. G. J. I. J. o. S.-S. C. An implantable 455-active-electrode 52-channel CMOS neural probe. *IEEE Journal of Solid-State Circuits* **2013**, 49, 248-261.
- [13] Lopez, C. M.;Mitra, S.;Putzeys, J.;Raducanu, B.;Ballini, M.;Andrei, A.;Severi, S.;Welkenhuysen, M.;Van Hoof, C.; Musa, S. 22.7 a 966-electrode neural probe with 384 configurable channels in 0.13 µm soi cmos. In 2016 IEEE International Solid-State Circuits Conference (ISSCC); IEEE, 2016; pp 392-393.
- [14] Seidl, K.;Schwaerzle, M.;Ulbert, I.;Neves, H. P.;Paul, O.; Ruther, P. J. J. o. m. s. CMOS-based high-density silicon microprobe arrays for electronic depth control in intracortical neural recording—characterization and application. *Journal of microelectromechanical systems* **2012**, *21*, 1426-1435.
- [15] Raducanu, B. C.; Yazicioglu, R. F.; Lopez, C. M.; Ballini, M.; Putzeys, J.; Wang, S.; Andrei, A.; Welkenhuysen, M.; Van Helleputte, N.; Musa, S. Time multiplexed active neural probe with 678 parallel recording sites. In 2016 46th European Solid-State Device Research Conference (ESSDERC); IEEE, 2016; pp 385-388.
- [16] Du, J.;Blanche, T. J.;Harrison, R. R.;Lester, H. A.; Masmanidis, S. C. J. P. o. Multiplexed, high density electrophysiology with nanofabricated neural probes. *PloS one* **2011**, *6*, e26204.
- [17] Tran, N.; Yang, J.; Bai, S.; Ng, D.; Halpern, M.; Grayden, D.; Skafidas, E.; Mareels, I. A fully flexible stimulator using 65 nm cmos process for 1024-electrode epi-retinal prosthesis. In 2009 Annual International Conference of the IEEE Engineering in Medicine and Biology Society; IEEE, 2009; pp 1643-1646.
- [18] Drake, K. L.; Wise, K. D.; Farraye, J.; Anderson, D. J.; BeMent, S. L. J. I. T. o. B. E. Performance of planar multisite microprobes in recording extracellular single-unit intracortical activity. *IEEE Transactions on Biomedical Engineering* **1988**, *35*, 719-732.

- [19] Kozai, T. D.;Du, Z.;Gugel, Z. V.;Smith, M. A.;Chase, S. M.;Bodily, L. M.;Caparosa, E. M.;Friedlander, R. M.; Cui, X. T. J. J. o. n. m. Comprehensive chronic laminar single-unit, multi-unit, and local field potential recording performance with planar single shank electrode arrays. *Journal of neuroscience methods* **2015**, *242*, 15-40.
- [20] Cogan, S. F. Neural stimulation and recording electrodes. *Annu Rev Biomed Eng* **2008**, *10*, 275-309.
- [21] Alba, N. A.; Du, Z. J.; Catt, K. A.; Kozai, T. D.; Cui, X. T. In Vivo Electrochemical Analysis of a PEDOT/MWCNT Neural Electrode Coating. *Biosensors* **2015**, *5*, 618-646.
- [22] Prasad, A.; Sanchez, J. C. J. J. o. n. e. Quantifying long-term microelectrode array functionality using chronic in vivo impedance testing. *Journal of neural engineering* **2012**, *9*, 026028.
- [23] Harrison, R. R.; Charles, C. J. I. J. o. s.-s. c. A low-power low-noise CMOS amplifier for neural recording applications. *IEEE Journal of solid-state circuits* **2003**, *38*, 958-965.
- [24] Scholten, K.; Larson, C. E.; Xu, H.; Song, D.; Meng, E. J. J. o. M. S. A 512-Channel Multi-Layer Polymer-Based Neural Probe Array. *Journal of Microelectromechanical Systems* **2020**, *29*, 1054-1058.
- [25] Wei, X.;Luan, L.;Zhao, Z.;Li, X.;Zhu, H.;Potnis, O.; Xie, C. J. A. S. Nanofabricated Ultraflexible Electrode Arrays for High Density Intracortical Recording. *Advanced Science* **2018**, *5*, 1700625.
- [26] Li, L.;Bowler, N.;Hondred, P.; Kessler, M. Dielectric response of polyimide to thermal and saline degradation. In 2010 Annual Report Conference on Electrical Insulation and Dielectic Phenomena; IEEE, 2010; pp 1-4.
- [27] Le Floch, P.; Molinari, N.; Nan, K.; Zhang, S.; Kozinsky, B.; Suo, Z.; Liu, J. J. N. L. Fundamental limits to the electrochemical impedance stability of dielectric elastomers in bioelectronics. *Nano Letters* **2019**, *20*, 224-233.
- [28] Chun, W.; Chou, N.; Cho, S.; Yang, S.; Kim, S. J. P. i. O. C. Evaluation of submicrometer parylene C films as an insulation layer using electrochemical impedance spectroscopy. *Progress in Organic Coatings* **2014**, *77*, 537-547.
- [29] Neto, J. P.;Baião, P.;Lopes, G.;Frazão, J.;Nogueira, J.;Fortunato, E.;Barquinha, P.; Kampff, A. R. J. F. i. n. Does impedance matter when recording spikes with polytrodes? *Frontiers in neuroscience* **2018**, *12*, 715.
- [30] Qiang, Y.;Seo, K. J.;Zhao, X.;Artoni, P.;Golshan, N. H.;Culaclii, S.;Wang, P. M.;Liu, W.;Ziemer, K. S.; Fagiolini, M. J. A. F. M. Bilayer nanomesh structures for transparent recording and stimulating microelectrodes. *Advanced Functional Materials* **2017**, *27*, 1704117.

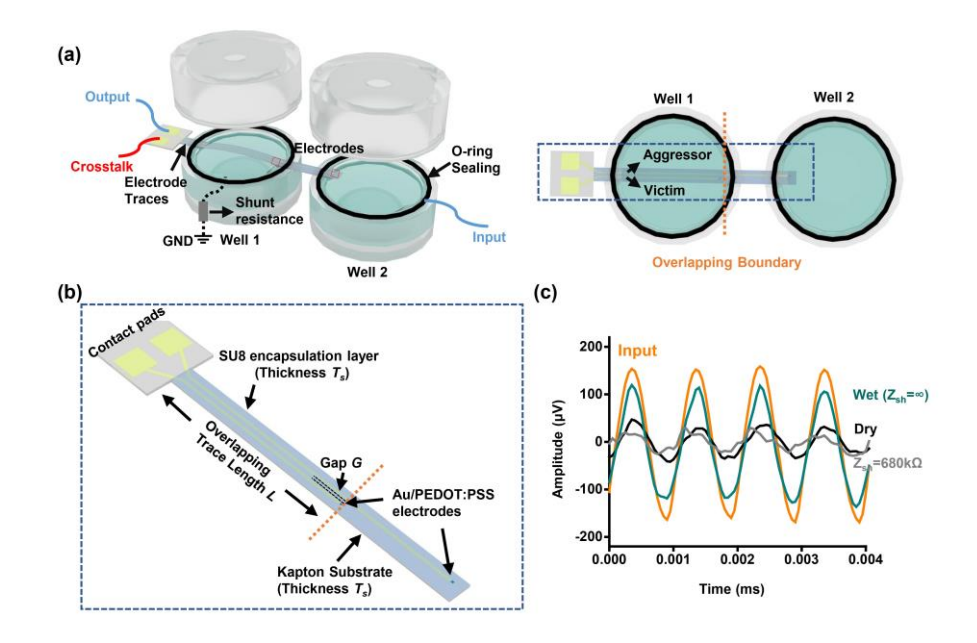
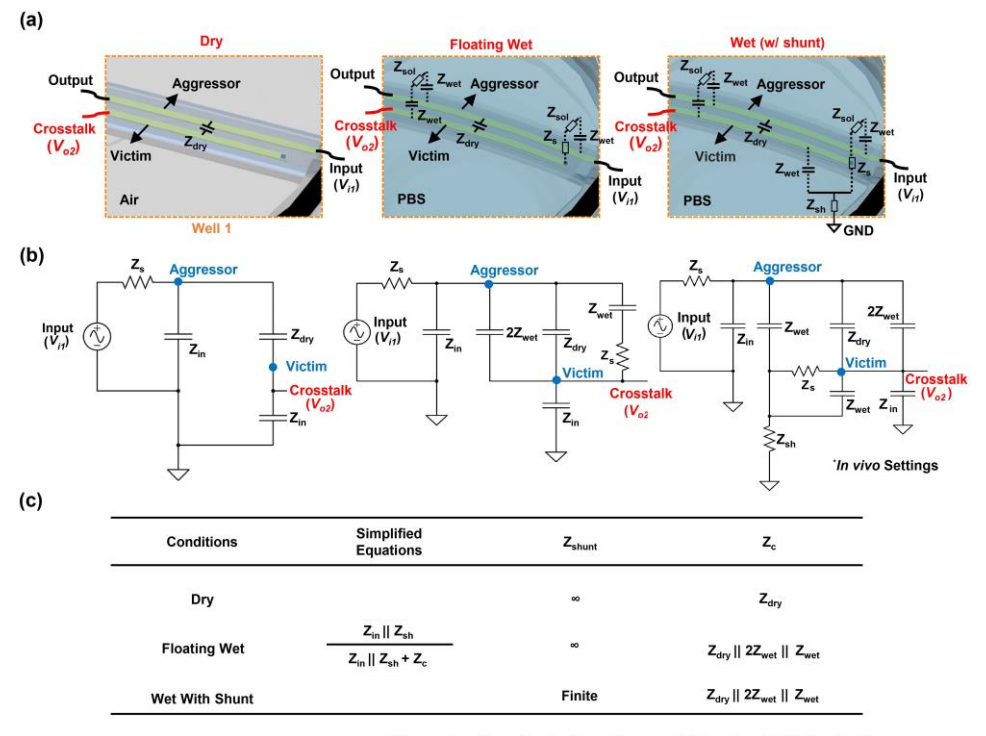


Figure 1. Crosstalk measurements of a polymer MEA using a two-well setup for wet conditions. (a) Illustration of the crosstalk measurement wet setup. (b) Electrodes configuration for the crosstalk measurement. (c) Measured crosstalk waveform in different environments compared to the input signal (black).



*Assumption: $Z_s \ll Z_{in}$, $Z_s \ll Z_{wet}$, Z_{sol} is negligible. Crosstalk(CT) = V_{oz}/V_{in}

Figure 2. Circuit modelling of the crosstalk under different measurement condition. (a)

Illustration of the 2-electrode crosstalk measurement circuits and components. Z_{dry} : coupling impedance between the two traces in air ambient. Z_{wet} : coupling impedance between the trace and the wet medium through encapsulation. Z_{sh} : shunt resistance from a single electrode to the ground. Z_{sol} : solution resistance of the wet medium. Z_{in} : Input impedance from the data acquisition system. Z_s : site impedance of the microelectrode. (b) Equivalent circuits of the crosstalk measurement setup. (c) Table of simplified equations to calculate crosstalk in different conditions. Z_c : Total coupling impedance between the 2 electrodes.

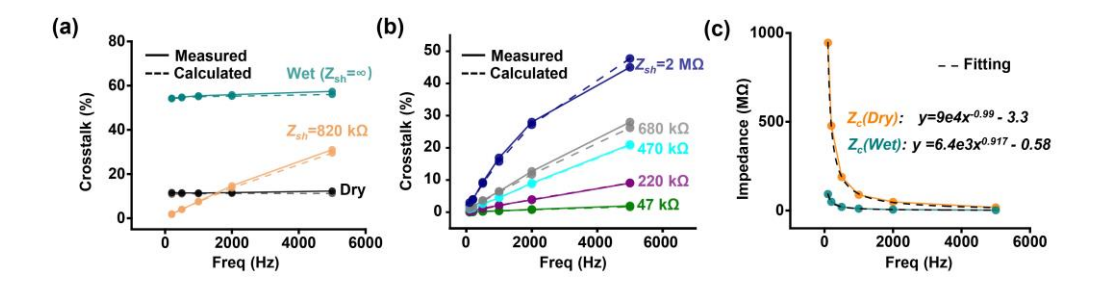


Figure 3. Dependence of crosstalk results on measurement conditions and device parameters. (a) The frequency spectrum of measured and calculated crosstalk in dry, floating wet and wet w/ shunt conditions. Solid line: measured crosstalk; Dashed line: calculated crosstalk using measured coupling impedance (Z_{dry} , Z_c). (b) Measured and calculated crosstalk with different shunt resistance. Solid line: measured crosstalk; Dashed line: calculated crosstalk using measured coupling impedance (Z_{dry} , Z_c). (c) Frequency spectrum of the coupling impedance Z_{dry} and Z_c . Dashed line: fitting curves, fitted equations shown in the panel. Electrode trace width: 100 μ m, trace overlap length: 14 mm.

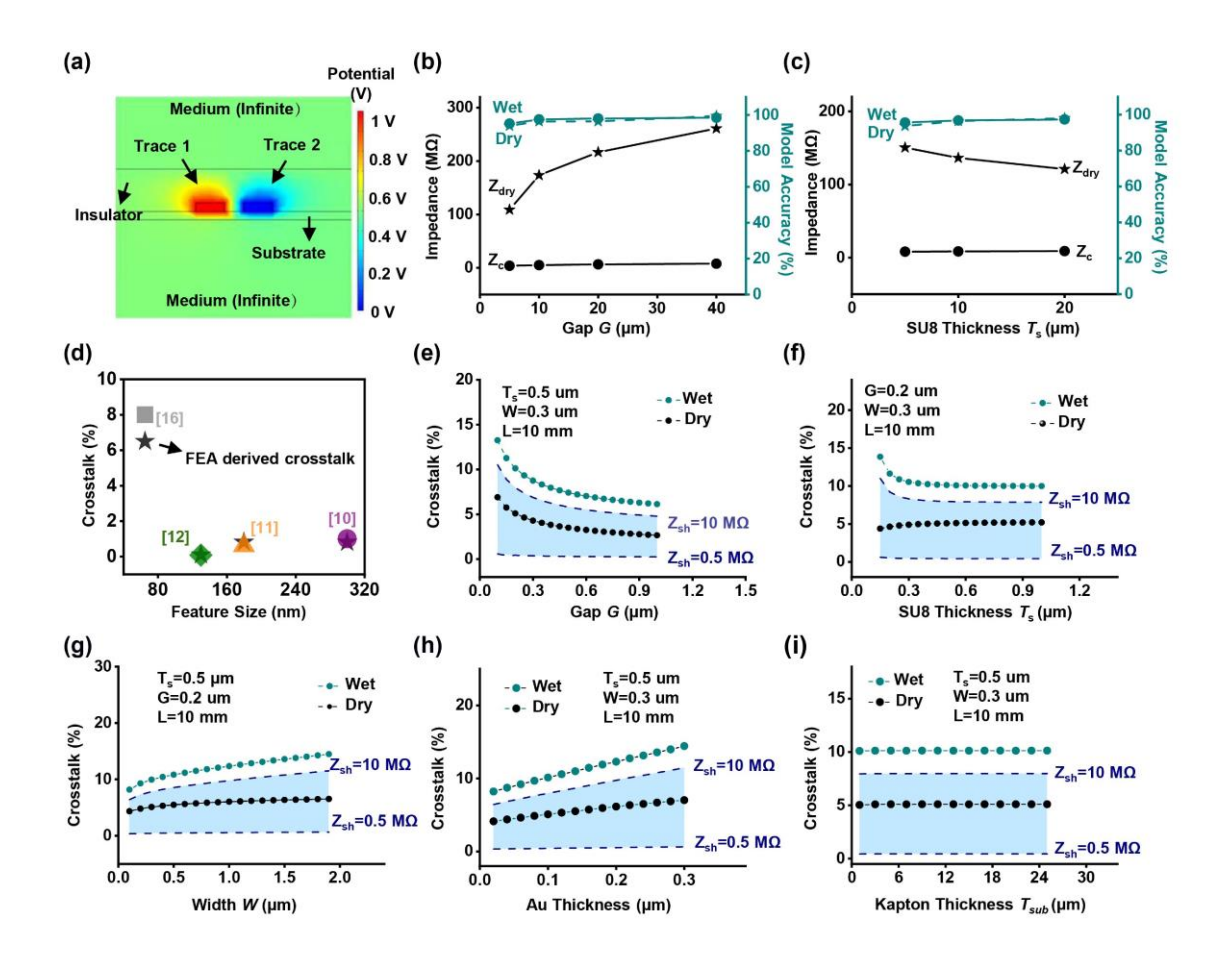


Figure 4. Coupling impedance simulation and crosstalk projection. (a) Simulation Model built in COMSOL with electrostatic potential mapping. (b) Simulated coupling impedance as a function of the gap between the 2 electrode traces in different conditions, with derived crosstalk model accuracy compared to the measured values. *Left axis*: Simulated coupling impedance; *Right axis: Crosstalk model accuracy*. (c) Simulated coupling impedance as a function of the thickness of encapsulation layer (SU8) in different conditions, with derived crosstalk model accuracy compared to the measured values. *Left axis*: Simulated coupling impedance; *Right axis: Crosstalk model accuracy*. (d) Comparison between the crosstalk values reported from the state-of-art Si probes and the simulated values using our model. The black stars denote the simulated values[10-12, 16]. (e) FEA derived crosstalk as a function of trace gaps in nanoscale devices. *Blue region*: crosstalk with shunt resistance ranging from 0.5 to 10 MΩ. (f) FEA derived crosstalk as a function of the encapsulation layer (SU8) thickness in nanoscale devices. *Blue region*: crosstalk with shunt resistance ranging from 0.5 to 10 MΩ. (g) FEA derived

crosstalk as a function of the Au trace widths in the nanoscale devices. (h) FEA derived crosstalk as a function of the Au trace thickness in the nanoscale devices. (i) FEA derived crosstalk as a function of the substrate thickness in the nanoscale devices. Blue region: crosstalk with shunt resistance ranging from 0.5 to $10 \text{ M}\Omega$.